Prepared for submission to JCAP

Inference of Love-Q Relations with Gravitational Waves in Hierarchical Bayesian Framework

Zhihao Zheng,[a]

[a]School of Yuanpei, Peking University, Beijing 100871, China
[b]Department of Astronomy, School of Physics, Peking University, Beijing 100871, China
[c]Kavli Institute for Astronomy and Astrophysics, Peking University, Beijing 100871, China
[d]Max Planck Institute for Gravitational Physics (Albert Einstein Institute), Am Mühlenberg 1, D-14476 Potsdam-Golm, Germany
[e]National Astronomical Observatories, Chinese Academy of Sciences, Beijing 100012, China

E-mail: 2300017794@stu.pku.edu.cn

Abstract. Nuclear and gravity theories have predicted a universal relation between the tidal deformability Λ and quadrupole moment Q of neutron stars, offering a robust method for testing gravity. However, this Love-Q relation has not yet been directly measured through astrophysical observations. The detection of gravitational wave (GW) event GW170817 provided a new channel for probing this relation, as both Λ and Q enter the GW waveform and can be inferred through parameter estimation. The next-generation GW detectors are expected to yield more GW observations with higher precision, enabling a measurement of the Love-Q relation. In this study, we construct a hierarchical Bayesian framework to conduct a systematic and efficient inference using simulated GW signals, aiming to determine the precision with which the Love-Q relation can be constrained. Our findings indicate that the results are dominated by the GW events with the highest signal-to-noise ratios and that a linear Love-Q model is sufficient for our dataset size. We also report a correlation in the posterior distribution of the parameters characterizing the Love-Q relation. Furthermore, our results suggest that dynamical Chern-Simons gravity can be constrained to $\xi_{\rm CS}^{1/4} < \mathcal{O}(10^2)$km, which is in agreement with the conclusion of previous studies.

Contents

1 Introduction

Neutron stars (NSs) serve as natural laboratories for testing nuclear and gravitational physics due to their extreme densities and strong gravitational fields—conditions unattainable in terrestrial and Solar System experiments. On the one hand, for nuclear physics, observations of NSs help us probe the equation of state (EOS) of high-density nuclear matter [1]. For instance, the EOS can be constrained by the observed maximum NS mass [2, 3] or the mass-radius relation [4–8]. On the other hand, modified gravity theories predict variations in the interior structure of NSs and their corresponding observable properties [9, 10]. By measuring these properties, constraints can be placed on different gravity theories.

However, current observations do not have enough precision to determine the actual EOS. Consequently, attempts to test modified gravity theories are complicated by a degeneracy between the effects of modified gravity and the uncertainties in EOS [10–12]. To break this degeneracy, Yagi and Yunes [11, 13] proposed using universal relations among NS properties, including the moment of inertia (I), tidal Love number (or tidal deformability Λ), and the dimensionless spin-induced quadrupole moment (Q). These I-Love-Q relations are EOS-insensitive (with variation of about 1% or less) yet they can be dependent on the underlying gravity theory. Hence, by independently measuring any two of the I-Love-Q trio, one can test gravity theories avoiding the degeneracy with the uncertainties from nuclear physics.

The recent observation of GW170817 demonstrated that gravitational waves (GWs) emitted during binary neutron star (BNS) coalescences have opened up a new observational window for investigating NS properties [14–16]. In a BNS system, tidal deformation occurs to each star due to the gravitational field of its companion [17, 18]. This interaction influences the inspiral of the binary, thereby leaving a distinct signature on the emitted GWs [19–23]. The effect is characterized by the tidal deformability $\Lambda = 2k_2/(3C^5)$, where k_2 is the tidal

Love number and C is the NS compactness [24]. Besides, a rotating NS experiences another deformation due to its spin, which induces a quadrupole moment $\mathcal{Q} = -Q\chi^2 m^3$ (spin-induced quadrupole moment, SIQM), where Q is the dimensionless quadrupole moment, [1] χ is the NS dimensionless spin and m is the NS mass [25, 26]. Similar to tidal deformability, the quadrupole moment also enters the GW waveform [27–30] and is therefore a key parameter to probe the properties of compact binaries with GW signals [31–34].

Future next-generation ground-based GW detectors, including the Cosmic Explorer (CE) [35, 36] and the Einstein Telescope (ET) [37–39], will detect much more GW signals (up to about 10^5–10^6 events per year) [40–43] and more precise measurements of the tidal deformability and the quadrupole moment [13, 44], thanks to their increased sensitivity and lower cutoff frequencies. With more high-precision GW data, one can combine the measurements of Λ and Q to infer the Love-Q relation from GW observations. While Samajdar and Dietrich [44] have performed a preliminary analysis concluding that the next-generation GW detectors will allow for a measurement of this relation, a more systematic and efficient framework is needed to join a considerable number of GW events and provide a robust estimation of the Love-Q relation.

Hierarchical Bayesian inference presents an appropriate method for this problem and has been applied in population analyses and EOS constraints [7, 45–51]. In our case, the Love-Q relation parameters can be regarded as the hyper parameters, and in hierarchical Bayesian framework, the inference of these hyper parameters is separated from the inference of the GW waveform parameters to achieve a higher level of computational efficiency.

In this work, we construct such a hierarchical Bayesian framework to infer the Love-Q relation from simulated GW signals, exploring its potential for combining future GW observations with next-generation detectors. We also investigate how the results are impacted by the number of GW events analysed and by the specific parameterization of Love-Q relation. Furthermore, as a direct application of our results, we discuss how the inferred Love-Q relation can be used to place constraints on dynamical Chern-Simons gravity.

This paper is organized as follows. In section 2 we construct the hierarchical Bayesian framework and derive the posterior of the hyper parameters. The simulation procedure is explained in detail in section 3. Then we present the results of our inference and discuss the inpact from different Love-Q relation parameterizations in section 4. We compare our inference results with the predictions of the dynamical Chern-Simons gravity as a test in section 5. Finally, we conclude this work in section 6.

2 Hierarchical Bayesian Inference of Love-Q Relation Parameters

2.1 Preliminary

In our simulation, we parameterize the Love-Q relation in linear (2-d) and quartic polynomial (5-d) manners as follows

$$\ln Q_{5d} = a_5 + b_5 \ln\Lambda + c_5 \ln^2\Lambda + d_5 \ln^3\Lambda + e_5 \ln^4\Lambda\,, \tag{2.1a}$$

$$\ln Q_{2d} = a_2 + b_2 \ln\Lambda\,. \tag{2.1b}$$

For the Yagi-Yunes relation, we have $a_5 = 0.1940$, $b_5 = 0.09163$, $c_5 = 0.04812$, $d_5 = -4.283 \times 10^{-3}$, and $e_5 = 1.245 \times 10^{-4}$ [52]. In figure 1, we plot the Yagi-Yunes relation as well as its

[1] We only talk about the dimensionless quadrupole moment later in the text and for simplicity, we ref Q as quadrupole moment without causing ambiguity.

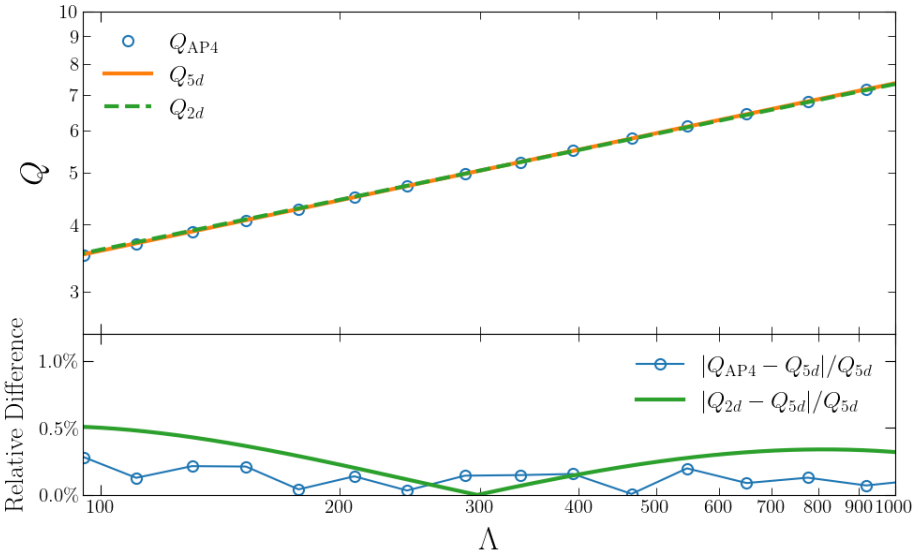

Figure 1: The upper panel shows the relation between $\ln \Lambda$ and $\ln Q$ for the Yagi-Yunes relation (5-d) and its linear fit (2-d). The lower panel shows the relative difference of 5-d and 2-d results.

linear fit and in this case, the relative difference in $\ln Q$ between these two parameterization manners is within $\mathcal{O}(1)\%$. No matter how we parameterize the Love-Q relation, these fitting coefficients do not enter the GW waveform and therefore cannot be directly measured from GW signals. Instead, different combinations of fitting coefficients determine different Love-Q relations, leading to an impact on the GW signals. In other words, such a Love-Q relation provides a delta-function-type prior for GW parameters Λ_i and Q_i. Correspondingly, the fitting coefficients of our Love-Q relation can be regarded as hyper parameters, denoted as $\boldsymbol{H}$. Then we write down the conditional prior

$$\pi(Q_i|\Lambda_i, \boldsymbol{H}) = \delta(Q_i - f(\Lambda_i; \boldsymbol{H}))\,. \tag{2.2}$$

2.2 Derivation

Hierarchical Bayesian inference is a framework that allows us to go beyond single GW events, joining a set of single events together to probe the Love-Q relation. In this framework, our main objective is to derive the posterior density function (PDF) $p(\boldsymbol{H}|D)$ for the fitting coefficients of the Love-Q relation, i.e. the hyper parameters. The data $D = \{\boldsymbol{d}_1, ..., \boldsymbol{d}_n\}$ contains data streams $\boldsymbol{d}_i$ of n GW events from the detector network. Note that we make no assumptions of EOS in the hierarchical Bayesian inference part and EOS does not emerge in the conditional probability functions, given that the Love-Q relation is EOS-insensitive. To acquire the marginalized posterior for only hyper parameters, we marginalize over the entire parameter space

$$p(\boldsymbol{H}|D) = \int p(\boldsymbol{H}, \boldsymbol{\theta}_1, ..., \boldsymbol{\theta}_n|D)\mathrm{d}\boldsymbol{\theta}_1 ... \mathrm{d}\boldsymbol{\theta}_n\,. \tag{2.3}$$

Then applying Bayes' theorem

$$p(\boldsymbol{H}, \boldsymbol{\theta}_1, ..., \boldsymbol{\theta}_n|D) = \pi(\boldsymbol{H}, \boldsymbol{\theta}_1, ..., \boldsymbol{\theta}_n)\frac{p(D|\boldsymbol{H}, \boldsymbol{\theta}_1, ..., \boldsymbol{\theta}_n)}{p(D)}\,, \tag{2.4}$$

where $\pi(\boldsymbol{H}, \boldsymbol{\theta}_1, ..., \boldsymbol{\theta}_n)$ is the prior probability density for the fitting coefficients and waveform parameters, $p(D|\boldsymbol{H}, \boldsymbol{\theta}_1, ..., \boldsymbol{\theta}_n)$ is the likelihood function, and $p(D)$ is the evidence which we do not need to calculate. Then we derive the prior and likelihood as follows.

Prior Considering the fact that the n events are independent, the prior can be decomposed into parts of hyper parameters and waveform parameters using the product rule of probability $p(A, B) = p(A)p(B|A)$

$$\pi(\boldsymbol{H}, \boldsymbol{\theta}_1, ..., \boldsymbol{\theta}_n) = \pi(\boldsymbol{H}) \prod_{i=1}^{n} \pi(\boldsymbol{\theta}_i|\boldsymbol{H}) \,. \tag{2.5}$$

We divide the set of waveform parameters for each event $\boldsymbol{\theta}_i$ into three categories: the tidal deformability parameters $\boldsymbol{\Lambda}_i = \{\Lambda_{1i}, \Lambda_{2i}\}$, the quadrupole moment parameters $\boldsymbol{Q}_i = \{Q_{1i}, Q_{2i}\}$, and the nuisance parameters $\boldsymbol{\xi}_i$. Since no particular EOS is chosen here, the $m - \Lambda$ relation remains undetermined. Therefore, we assume that the prior distributions for nuisance parameters, including the two mass parameters, are independent of $\boldsymbol{\Lambda}_i, \boldsymbol{Q}_i$ and $\boldsymbol{H}$. In this way, the conditional prior for the waveform parameters in eq. (2.5) can be further decomposed with the product rule

$$\pi(\boldsymbol{\theta}_i|\boldsymbol{H}) = \pi(\boldsymbol{\Lambda}_i|\boldsymbol{H})\pi(\boldsymbol{Q}_i|\boldsymbol{\Lambda}_i, \boldsymbol{H}) \times \pi(\boldsymbol{\xi}_i) \,. \tag{2.6}$$

Likelihood Analogously, we decompose the likelihood into a product of single-event likelihoods for n independent BNS observations

$$p(D|\boldsymbol{H}, \boldsymbol{\theta}_1, ..., \boldsymbol{\theta}_n) = \prod_{i=1}^{n} p(\boldsymbol{d}_i|\boldsymbol{H}, \boldsymbol{\theta}_i) \tag{2.7a}$$

$$= \prod_{i=1}^{n} p(\boldsymbol{d}_i|\boldsymbol{\theta}_i) \,. \tag{2.7b}$$

Note that in the second line we have used the fact that the hyper parameters do not enter the waveform thus the likelihood only depends on $\boldsymbol{\theta}_i$, i.e. $p(\boldsymbol{d}_i|\boldsymbol{H}, \boldsymbol{\theta}_i) = p(\boldsymbol{d}_i|\boldsymbol{\theta}_i)$.

Based on the derivation above, now the marginalized PDF (eq. (2.3)) is

$$\begin{aligned} p(\boldsymbol{H}|D) &= \frac{1}{p(D)}\pi(\boldsymbol{H}) \int \mathrm{d}\boldsymbol{\theta}_1 ... \mathrm{d}\boldsymbol{\theta}_n \prod_{i=1}^{n} \left[\pi(\boldsymbol{\Lambda}_i|\boldsymbol{H})\pi(\boldsymbol{Q}_i|\boldsymbol{\Lambda}_i, \boldsymbol{H})\pi(\boldsymbol{\xi}_i)p(\boldsymbol{d}_i|\boldsymbol{\theta}_i)\right] \\ &= \frac{1}{p(D)}\pi(\boldsymbol{H}) \prod_{i=1}^{n} \int \mathrm{d}\boldsymbol{\Lambda}_i \mathrm{d}\boldsymbol{Q}_i \pi(\boldsymbol{\Lambda}_i|\boldsymbol{H}) \delta\left(\boldsymbol{Q}_i - \boldsymbol{f}(\boldsymbol{\Lambda}_i; \boldsymbol{H})\right) \int \mathrm{d}\boldsymbol{\xi}_i \pi(\boldsymbol{\xi}_i) p(\boldsymbol{d}_i|\boldsymbol{\theta}_i) \\ &= \frac{1}{p(D)}\pi(\boldsymbol{H}) \prod_{i=1}^{n} \int \mathrm{d}\boldsymbol{\Lambda}_i \pi(\boldsymbol{\Lambda}_i|\boldsymbol{H}) L_i\left(\boldsymbol{\Lambda}_i, \boldsymbol{f}(\boldsymbol{\Lambda}_i; \boldsymbol{H})\right) \,. \end{aligned} \tag{2.8}$$

where we define the quasi-likelihood function for $\boldsymbol{\Lambda}_i, \boldsymbol{Q}_i$ as

$$L_i(\boldsymbol{\Lambda}_i, \boldsymbol{Q}_i) = \int \mathrm{d}\boldsymbol{\xi}_i \pi(\boldsymbol{\xi}_i) p(\boldsymbol{d}_i|\boldsymbol{\theta}_i) \,. \tag{2.9}$$

What we need to compute now are the quasi-likelihood functions (eq. (2.9)) for each GW event and then substitute them into eqs. (2.8). In hierarchical Bayesian inference, these quasi-likelihood functions can be calculated in advance to reduce computational cost,

considering that the hyper parameters $\boldsymbol{H}$ do not appear in eq. (2.9) [7, 53, 54]. We start from Bayes' theorem for the i-th GW event

$$p(\boldsymbol{\theta}_i|\boldsymbol{d}_i) \propto \pi(\boldsymbol{\theta}_i|\varnothing)p(\boldsymbol{d}_i|\boldsymbol{\theta}_i)\,, \tag{2.10}$$

where $\pi(\boldsymbol{\theta}_i|\varnothing)$ is the default prior chosen as long as it is sufficiently uninformative[53], and $p(\boldsymbol{d}_i|\boldsymbol{\theta}_i)$ is the single-event likelihood [55],

$$p(\boldsymbol{d}_i|\boldsymbol{\theta}_i) \propto \mathrm{e}^{-\frac{1}{2}\langle d_i - h(\boldsymbol{\theta}_i), d_i - h(\boldsymbol{\theta}_i)\rangle}\,. \tag{2.11}$$

$h(\boldsymbol{\theta}_i)$ is given by the waveform model in section 2.1 while $\langle g, h\rangle$ is the inner product of $g(t)$ and $h(t)$ weighted by the power spectrum density(PSD) of $S_n(f)$ of the noise.

$$\langle g, h\rangle := 2\mathrm{Re}\int_{-\infty}^{\infty} \frac{\tilde{g}^*(f)\tilde{h}(f)}{S_n(|f|)}\mathrm{d}f\,, \tag{2.12}$$

where $\tilde{g}(f)$ and $\tilde{h}(f)$ are the Fourier transforms of $g(t)$ and $h(t)$.

What we choose for the default prior in eq. (2.10) is not so important as long as it is sufficiently uninformative [53]. Rearranging terms of eq. (2.10) and substituting it into eq. (2.9), we obtain

$$\begin{aligned} L_i(\boldsymbol{\Lambda}_i, \boldsymbol{Q}_i) &= \int \mathrm{d}\boldsymbol{\xi}_i \pi(\boldsymbol{\xi}_i) p(\boldsymbol{d}_i|\boldsymbol{\theta}_i) \\ &\propto \int \mathrm{d}\boldsymbol{\xi}_i \frac{\pi(\boldsymbol{\xi}_i)}{\pi(\boldsymbol{\theta}_i|\varnothing)} p(\boldsymbol{\theta}_i|\boldsymbol{d}_i)\,, \end{aligned} \tag{2.13}$$

which allows us to construct the quasi-likelihood function with posteriors of each event. In particular, as long as we choose flat priors for tidal and quadrupole moment parameters, the quasi-likelihood function is proportional to the marginalized posterior for every single event.

3 Simulation

3.1 Waveform, Population and Detectors

For our simulation, we adopt the IMRPHENOMXAS_NRTIDALV3 waveform model [30], which is an aligned spin waveform and includes tidal amplitude corrections as well as spin-induced quadrupole moment terms up to 3.5PN. The parameter set is composed of the binary masses m_1 and m_2, the dimensionless tidal deformabilities Λ_i and spin-induced quadrupole moments Q_i of each component, the dimensionless spin aligned with the direction of the orbital angular momentum χ_i, the luminosity distance to the source D_L, the merge time t_c, the right ascension α and declination δ, the inclination angle ι, the GW polarization angle ψ and the phase of coalescence ϕ_c. We denote the entire parameter set as a vector $\boldsymbol{\theta}$, i.e.

$$\boldsymbol{\theta} = \{m_1, m_2, \Lambda_1, \Lambda_2, Q_1, Q_2, \chi_1, \chi_2, D_L, t_c, \alpha, \delta, \iota, \psi, \phi_c\}\,. \tag{3.1}$$

Since our curiosity lies in tidal deformability and quadrupole moment, other parameters are regarded as nuisance parameters, which are denoted as $\boldsymbol{\xi}$.

We adopt the BNS mass population model proposed by Farrow et al. [56], in which the two BNS components do not necessarily have the same mass distribution. According to their spin magnitude, the model divides BNS into a recycled star and a nonrecycled (*slow*) one,

for which the masses are labeled m_r and m_s, respectively. The distribution of m_r has two Gaussian components while m_s follow a Uniform distribution,

$$P(m_r) = \alpha\mathcal{N}(\mu_1, \sigma_1) + (1-\alpha)\mathcal{N}(\mu_2, \sigma_2)\,, \tag{3.2a}$$

$$P(m_s) = \mathcal{U}(m_s^l, m_s^u)\,, \tag{3.2b}$$

where $\alpha = 0.68$, $\mu_1 = 1.34M_\odot$, $\sigma_1 = 0.02M_\odot$, $\mu_2 = 1.47M_\odot$, $\sigma_2 = 0.15M_\odot$ and $m_s^l = 1.14M_\odot$, $m_s^u = 1.46M_\odot$. When generating simulation GW signals, for each event we just select the larger one of m_r and m_s as the primary mass m_1 and the other as the secondary mass m_2, since we always demand $m_1 \geq m_2$.

The tidal deformability and quadrupole moments of the binary are calculated from the stellar mass, assuming the AP4 EOS, which is a soft EOS consistent with the LIGO-Virgo tidal measurements [14–16]. Refs. [13, 57] demonstrates in detail how to derive tidal deformability Λ_i and quadrupole moment Q_i given the mass m_i and the EOS. For the dimensionless spin component χ_r of recycled stars, we adopt a uniform distribution $\mathcal{U}(-0.5, 0.5)$, while in the case of slow stars, the spin χ_s is drawn from $\mathcal{U}(-0.1, 0.1)$.

Using the cosmological parameters provided by the Planck Collaboration [58], we simulate 1000 GW sources distributed uniformly in co-moving volume from 15Mpc to 150Mpc [50, 59], with isotropic sky locations and orientations. This corresponds to the observed local merger rate $R = 320^{+490}_{-270}\,\mathrm{Gpc}^{-3}\mathrm{yr}^{-1}$ from current GW detections [60]. To reduce the calculation cost, we only select sources with the highest signal-to-noise ratio (SNR) for Bayesian inference. Without loss of generality, all these GW events are injected with an arbitrary coalescence time $t_c = 0$.

A ground-based network consisting of two CE detectors and one ET detector is selected as the GW detectors. We simulate data in noise generated with designed sensitivity curves taken as CE-2 [35, 36] and ET-D [37–39]. The two CE detectors are positioned at the current sites of the two LIGO detectors, while the ET detector is set at the current location of the Virgo detector with a triangular shape. For these next-generation detectors, their lower cutoff frequencies $f_{\rm low}$ can reach about 1 Hz. Compared to $f_{\rm low} = 28$ Hz for advanced LIGO and Virgo, a smaller $f_{\rm low}$ means an improvement in both the signal-to-noise ratio and the duration when the signal is visible in band.

3.2 Implementation

The evaluation of the marginalized posterior for hyper parameters can be divided into two steps, similar to Refs. [5, 7, 51]. We first perform Bayesian inference for each event using some sampling methods, such as the Markov Chain Monte Carlo (MCMC) method [61, 62] and nested sampling [63, 64], generating posterior samples to acquire the quasi-likelihood (eq. (2.13)) through density estimation; then we substitute the quasi-likelihoods into eq. (2.8) to obtain the posterior of hyper parameters.

In the first step, when conducting single-event Bayesian inference, we choose $\mathcal{M}$ and η as mass parameters. In this way, the parameter set of single-event Bayesian inference becomes $\boldsymbol{\theta} = \{\mathcal{M}, \eta, \Lambda_1, \Lambda_2, Q_1, Q_2, \chi_1, \chi_2, D_L, t_c, \alpha, \delta, \iota, \psi, \phi_c\}$. The priors of $\mathcal{M}, \eta, \chi_1, \chi_2, t_c, \phi_c$ are uniform, while the prior of D_L is uniform in the co-moving volume and source frame time. Isotropy is ensured by setting priors for the angle variables $\alpha, \delta, \iota, \psi$. For tidal and quadrupole moment parameters, we treat Λ_s and Q_s of the slow binary component as nuisance parameters, considering that the spin-induced quadrupole moment is poorly estimated with low

spin [13]. And we select uniform priors for Λ_1, Λ_2 and Q_1, Q_2 so that eq. (2.13) can be further simplified as

$$\begin{aligned} L_i(\Lambda_{ri}, Q_{ri}) &\propto \int \mathrm{d}\boldsymbol{\xi}_i \frac{\pi(\boldsymbol{\xi}_i)}{\pi(\boldsymbol{\theta}_i|\varnothing)} p(\boldsymbol{\theta}_i|\boldsymbol{d}_i) \\ &\propto \int \mathrm{d}\boldsymbol{\xi}_i p(\boldsymbol{\theta}_i|\boldsymbol{d}_i) \\ &\propto p(\Lambda_{ri}, Q_{ri}|\boldsymbol{d}_i)\,, \end{aligned} \tag{3.3}$$

where Λ_{ri} and Q_{ri} are the tidal deformability and quadrupole moment of the recycled binary component of the ith event, respectively. Eq. (3.3) indicates that the quasi- likelihood is proportional to the marginalized posterior, revealing that we can directly construct the quasi-likelihood from posterior samples.

After sampling, we obtain the quasi-likelihood of each event from Λ_r and Q_r samples. To complete the integral in eq. (2.8), we must create a functional form for each quasi-likelihood using the posterior samples. Following Golomb and Talbot [54], we introduce the Gaussian mixture model (GMM) method developed by Ref. [65] as the density estimation method to obtain the quasi-likelihood with eq. (2.9). Substitute the results of density estimation into eq. (2.8), and then the likelihood function of the hyper parameter estimation can be constructed.

In the second step, we sample the integrand of eq. (2.8) with Bayesian inference. For hyper parameters $\pi(\boldsymbol{H})$, we use uniform priors with the boundaries listed in Table 1 and for the prior $\pi(\boldsymbol{\Lambda}_i|\boldsymbol{H})$, we use the uniform distribution $\mathcal{U}(10, 2000)$. For Bayesian inference in both steps, posterior samples are generated with NESSAI [66–68] of the BILBY [69] package. 20 simulated GW sources with the highest SNRs and spins are selected from 1000 sources, which are generated as described in section 3.1.

Table 1: The best fit values of Yagi-Yunes relation and the priors of the hyper parameters in linear and quartic polynomial fitting models for the Bayesian inference.

			Best fit values		
Parameter	a_i	b_i	c_i	d_i	e_i
5-d	0.1940	0.0916	4.812×10^{-2}	-4.283×10^{-3}	1.245×10^{-4}
4-d	0.1290	0.1480	3.021×10^{-2}	-1.817×10^{-3}	/
3-d	−0.0709	0.2775	3.220×10^{-3}	/	/
2-d	−0.1457	0.3094	/	/	/
			Prior		
Parameter	a_i	b_i	c_i	d_i	e_i
5-d	$\mathcal{U}(-5.0, 5.0)$	$\mathcal{U}(-1.0, 1.0)$	$\mathcal{U}(-0.5, 0.5)$	$\mathcal{U}(-0.1, 0.1)$	$\mathcal{U}(-0.01, 0.01)$
4-d	$\mathcal{U}(-5.0, 5.0)$	$\mathcal{U}(-1.0, 1.0)$	$\mathcal{U}(-0.5, 0.5)$	$\mathcal{U}(-0.1, 0.1)$	/
3-d	$\mathcal{U}(-5.0, 5.0)$	$\mathcal{U}(-1.0, 1.0)$	$\mathcal{U}(-0.5, 0.5)$	/	/
2-d	$\mathcal{U}(-5.0, 5.0)$	$\mathcal{U}(-1.0, 1.0)$	/	/	/

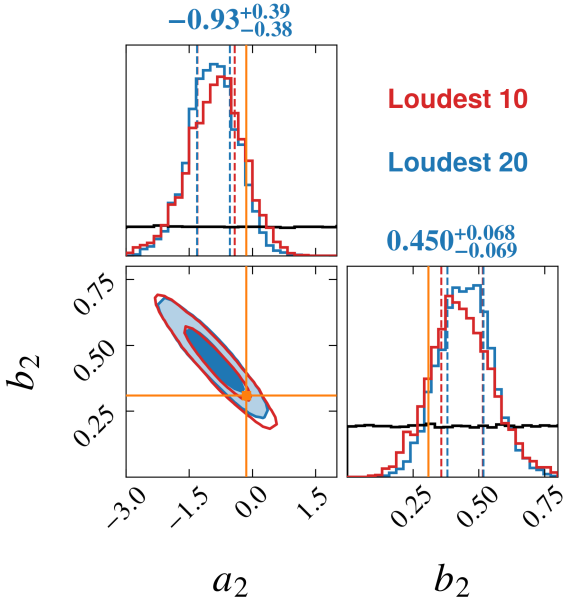

Figure 2: Posterior distributions of the hyper parameters in the linear fitting case. The contours refer to 50% and 90% credible regions for both inferences based on the loudest 10 and 20 events. The numbers above the histograms stand for the median and the central 50% credible interval of each marginalized distribution in the 20 event inference. The orange lines represent the best fit values of the parameters in Table. 1. The priors are also drawn in black for the histograms on the diagonal.

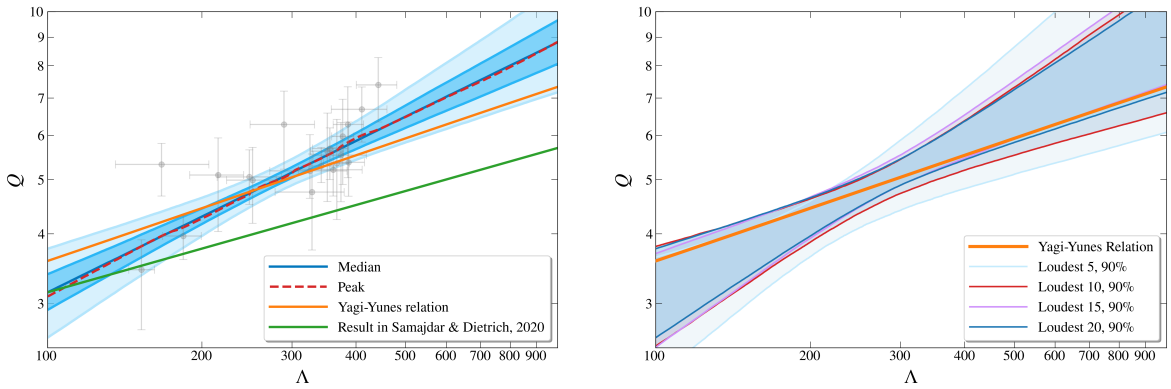

Figure 3: Results of the hierarchical Bayesian inference for linear Love-Q relation. In the left panel, the Love-Q relation is inferred based on 20 simulated GW events. The gray error bars demonstrate the 1σ credible interval of Λ and Q. The orange solid line represents the Yagi-Yunes Love-Q relation and the green solid line refs to the result given by Samajdar & Dietrich, 2020 [44]. The blue regions from dark to light represent the 50% and 90% credible intervals of Q. The blue solid line and the red dashed line are the median and peak of the distribution of Q with certain Λ. Note that the Yagi-Yunes Love-Q relation is covered within the 90% credible interval. In the right panel, contours correspond to 90% credible intervals for the inference result based on the loudest 5, 10, 15, 20 events, respectively.

4 Results and Discussions

4.1 Linear Fitting Model

Based on the methods discussed above, we perform the hierarchical Bayesian inference for linear Love-Q relations. Following Ref. [7], we show how the results depend on the number of events to verify if it is valid to select sources with the highest SNR (loudest) only. The posterior distributions for the hyper parameters of 10 event inference and 20 event inference are both demonstrated in figure. 2 as a comparison. For the joint distribution in the lower left corner, we find that the credible regions of the two inferences are quite similar, and the best fit values listed in Table. 1 are close to the edge of the 50% credible regions in the joint distribution. Moreover, in both cases, correlation exists between the two hyper parameters, since the credible regions are approximate oblique ellipses. In the diagonal corners, the peak values of the marginalized distributions for the two cases are also close to each other, indicating the dominance of events with higher SNR. An increase in the number of events just slightly narrows the peak width of the marginalized posteriors, and accordingly the 50% credible region shrinks in the loudest 20 events case.

In the left panel of figure. 3, we plot the linear Love-Q relation according to the posterior samples. For a certain Λ, every sample point of hyper parameters corresponds to a Q value. With Λ fixed, we find the 50% and 90% credible intervals of Q, and for continuously variable Λ, the intervals combine to form a region. As we can see, the Yagi-Yunes Love-Q relation is almost covered by the 90% region. The credible intervals are wide at both ends and narrow in the middle, as most of the events concentrate in the $\Lambda \sim 400$ region. In the right panel, we compare the credible regions for inferences using the loudest 5, 10, 15 and 20 events. The 90% regions for the latter three cases almost overlap each other. This means that the loudest 10 events dominate the results, and thus including much quieter events will not significantly improve the results.

4.2 Quartic Polynomial Fitting Model

For the quartic polynomial fitting model, we parameterize the Love-Q relation by eq. (2.1a) and perform a hierarchical Bayesian inference for five hyper parameter $\{a_5, b_5, c_5, d_5, e_5\}$. The left panel of figure 4 illustrates the posterior distributions of the hyper parameters for this 5-d model. Similarly to figure 2, the priors and marginalized posteriors are plotted together in the diagonal histograms. The values taken in Yagi-Yunes Love-Q relation are closed to the marginalized distribution peaks, which become consistent with the maximum likelihood estimation given flat priors. Compared to the linear fitting case, these peaks are wider in the prior space and thus the credible regions in the two-parameter joint distributions become broader. This is reasonable since the increase in the degree of freedom makes it harder to constrain each parameter.

We summarize the 5-d Love-Q relation constraining results in the right panel of figure 4 according to the posterior distributions. We mark the 50% and 90% credible intervals of Q using the same method as 2-d model. Like in figure 3 for linear Love-Q relations, the Yagi-Yunes relation almost falls within the 90% region. In addition, the widths of the 90% regions with $\Lambda \sim 400$ in figure 4 and figure 3 are close, except for the wider end in 5-d case when Λ is large. This is understandable because c_5, d_5 and e_5 are much smaller than a_5 and b_5, making the $\ln^k \Lambda$ terms with $k \leq 1$ dominate when Λ is not large enough.

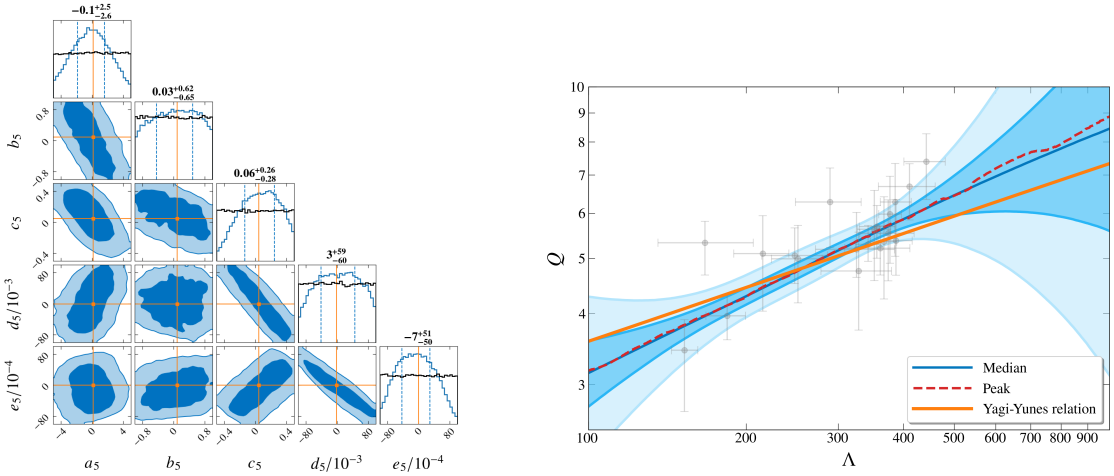

Figure 4: Left panel: posterior distribution of the hyper parameters in the quartic polynomial fitting case. The inference is based on all of the 20 events. The orange lines represent the values in the Yagi-Yunes Love-Q relation. Right panel: similar to figure. 3, but for the quartic polynomial fitting case. Still, the Yagi-Yunes Love-Q relation is included in the 90% credible region.

4.3 Discussion: More Fitting Models

We have mentioned in section 4.2 that it will be harder to constrain every hyper parameter as the degree of freedom increases, thus we perform hyper parameter inferences for quadratic and cubic polynomial, i.e. 3-d and 4-d, fitting models. Figure 5 demonstrates the posteriors and the corresponding Love-Q inference results for 3-d and 4-d models. In the 3-d case, we find strong degeneracy among the three parameters. The marginalized posterior distributions of a_3 and c_3 have very wide and flat peaks, while b_3 is so poorly constrained that its posterior is similar to its prior. When it comes to the 4-d inference results, degeneracy still emerges and again we find the marginalized posterior of one hyper parameter b_4 resemble the prior. These results imply that for our simulation data size, a 2-d linear fitting model is enough and the two fitting coefficients can be well constrained by our hierarchical Bayesian inference.

Same as before, we plot the constraint of Love-Q relation according to the posterior samples in the two lower panels of figure 5. Like 2-d and 5-d results, the width of the 90% region where most of the data points gather is insensitive to our parameterization of the Love-Q relation. We expect a better constraint to the both ends of the 90% regions based on more GW events, which may contain more information for the behavior of the Love-Q relation with $\Lambda \sim 100$ or $\Lambda > 500$.

5 Testing Modified Gravity: Dynamical Chern-Simons Gravity

For some parity-violating modified gravity theories that have not been stringently constrained yet, a I-Love-Q test can be powerful due to the significant difference in I-Love-Q relation emerging in these theories [52, 70]. We select the dynamical Chern-Simons (dCS) gravity [71–73] for discussion, considering that the I-Love-Q relation degeneracy only occurs in the limit when the coupling constant becomes infinitesimal [11, 13, 74]. By comparing the uncertainty given by our inference results with the deviation originating from the dCS gravity, we can see to what extent can our results constrain the coupling constants in dCS gravity at most.

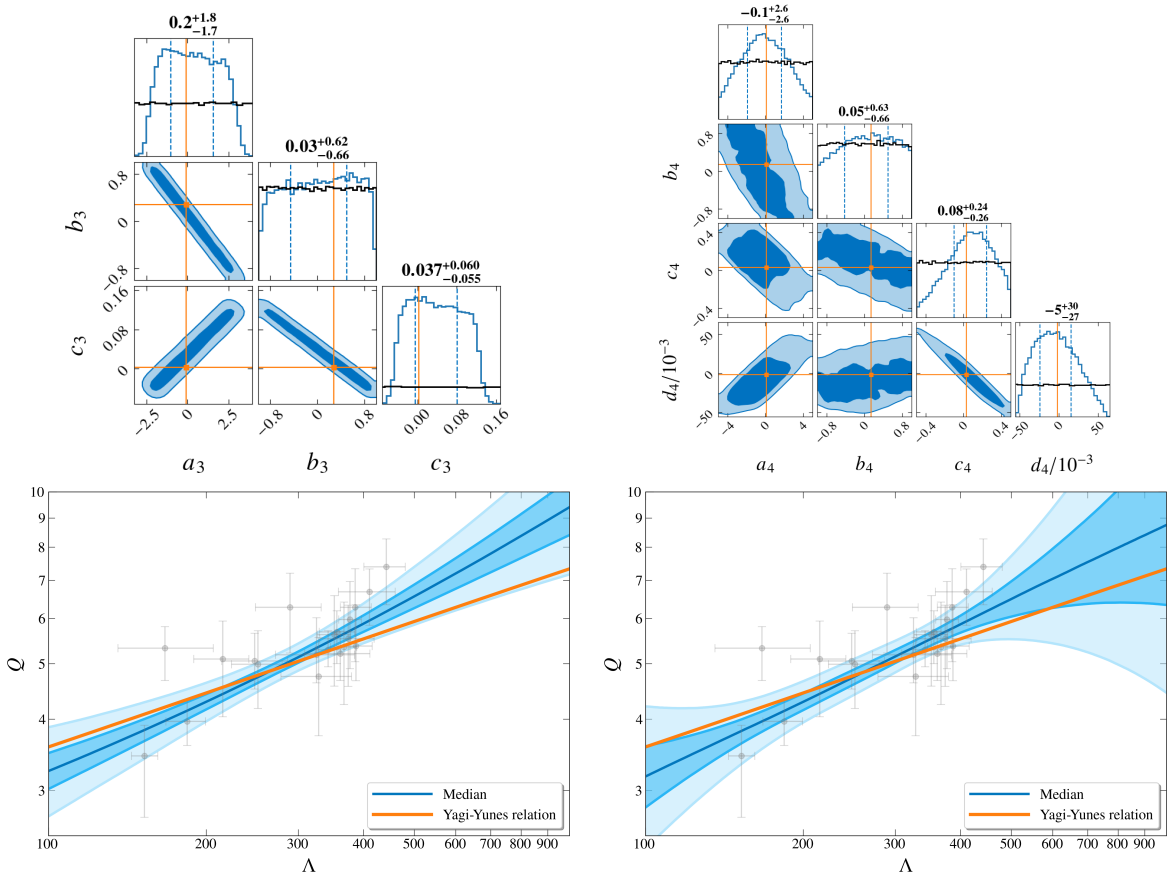

Figure 5: Results of quadratic and cubic polynomial (3-d and 4-d) fitting models. The two upper panels demonstrate the posteriors of the hyper parameters. And the best fit values (see table 1) are marked in orange. The two bottom panels present the inference results in Love-Q plane, similar to figure 3.

The dCS gravity introduces parity violation and quadratic curvature terms into the action [73, 74]

$$S = \int \mathrm{d}^4x\sqrt{-g}\left[\kappa_g\mathcal{R} + \frac{\alpha}{4}\vartheta\mathcal{R}_{\nu\mu\rho\sigma}{}^*\mathcal{R}^{\mu\nu\rho\sigma} - \frac{\beta}{2}(\nabla_\mu\vartheta\nabla^\mu\vartheta + 2V(\vartheta)) + \mathcal{L}_{\rm mat}\right], \tag{5.1}$$

where $\mathcal{R}$ is the Ricci scalar, $\mathcal{L}_{\rm mat}$ is the matter Lagrangian density, g is the determinant of the metric, $\kappa_g \equiv 1/(16\pi)$, and α and β are the coupling constants in dCS gravity. We assume that the pseudo-scalar field ϑ is dimensionless, thus the quantity $\xi_{\rm CS}^{1/4} \equiv [\alpha^2/(\kappa\beta)]^{1/4}$ can be regarded as a characteristic length scale of the theory. Current Solar System observations have constrained $\xi_{\rm CS}^{1/4} < \mathcal{O}(10^8)$km [75, 76].

For our Love-Q test, ref. [77] obtained the dCS correction to the NS quadrupole moment and ref. [78] indicates that the tidal deformability is the same as in GR at leading order in small coupling approximation $\zeta \equiv \xi_{\rm CS}M^2/R^6 \ll 1$, regarding the dCS gravity as an effective theory. Refs. [52, 77] have discussed the I-Love-Q relations under dCS gravity and find that the relations remain universal when we normalize the variables with respect to $\bar{\xi} \equiv \xi_{\rm CS}/M^4$, while become EOS-sensative with $\xi_{\rm CS}$ or ζ fixed.

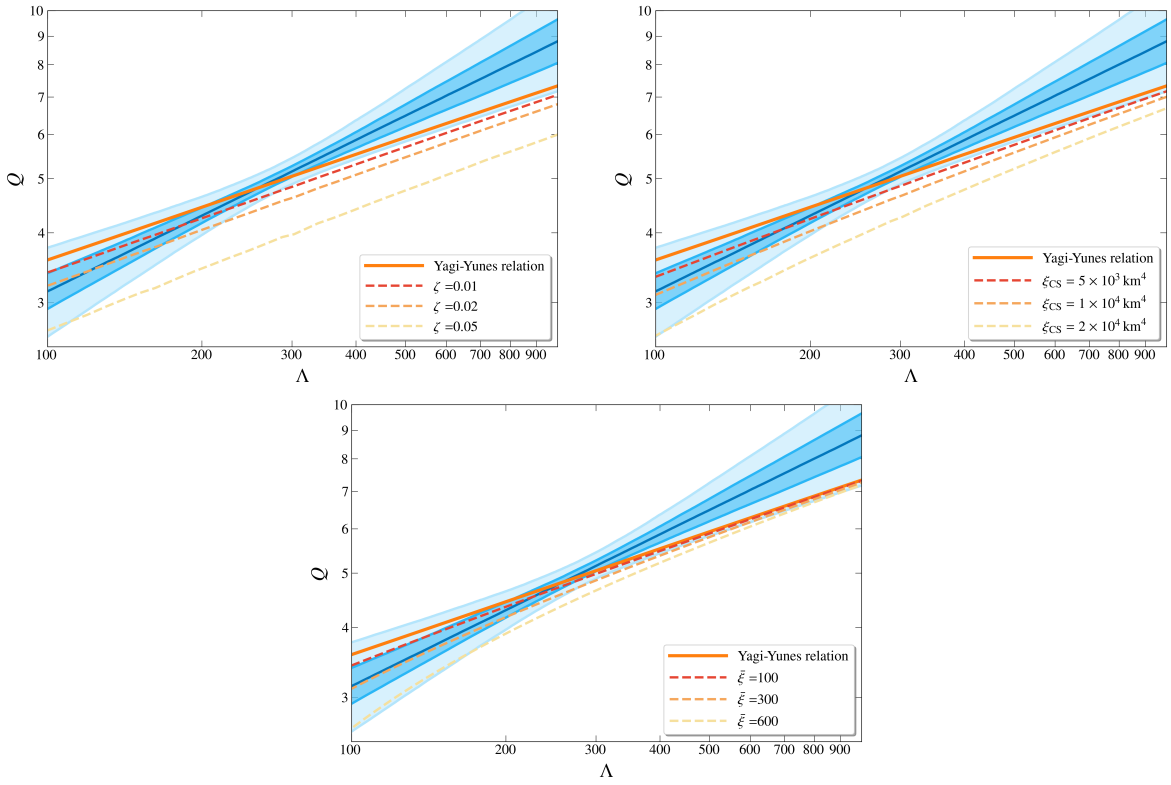

Figure 6: Comparison of the hierarchical inference results and CS predictions with different coupling constants fixed. The blue regions are the same as figure 3 (Linear fitting model). For each of the coupling constants of CS gravity $\zeta, \xi_{\rm CS}$ and $\bar{\xi}$, three possible values are taken and the corresponding Love-Q relations for AP4 EOS are drawn respectively as references.

Following ref. [52], we calculate the dCS Love-Q relation with $\zeta, \xi_{\rm CS}$ and $\bar{\xi}$ fixed respectively for the AP4 EOS, which has been assumed in our simulation in section 3. The results are demonstrated in figure 6. We compare the hierarchical Bayesian inference constraint of the Love-Q relation using linear fitting model (figure 3) with some possible Love-Q relations with respect to certain coupling constants in dCS gravity. From figure 6 we can conclude that our Love-Q test of dCS gravity can constrain the characteristic length $\xi_{\rm CS}^{1/4} < \mathcal{O}(10^2)$km, which is in agreement with the results given by refs. [11, 13].

6 Conclusion

This work has constructed a hierarchical Bayesian framework to estimate the Love-Q relation of NSs. By separating the single-event inferences and hyper parameter inference, this framework manifests high computational efficiency and provides a sophisticated statistical method for hyper parameter estimation. We applied this framework to simulated GW events for a next-generation detector network to examine the potential of constraining the Love-Q relation with GW observations. The results demonstrated that with the next-generation GW detector network, one can obtain a reliable measurement of the Love-Q relation through hierarchical Bayesian inference. We have also verified that the inference results of the hyper

parameters are dominated by events with the highest SNRs, which is consistent with the findings of ref. [7].

We then investigated the impact of different parameterizations for Love-Q relation on the inference. We found that constraint of the Love-Q relation is insensitive to the parameterization in the region where most data points gather. Also, as shown by the posterior distributions, degeneracies between hyper parameters exist in all cases studied. Furthermore, for all but the linear model, at least one hyper parameter was poorly constrained, exhibiting wide and flat posterior. These results indicate that a two-parameter (linear) model is sufficient for our data volume (20 GW events).

Finally, as a practical application, we compared our inference results with the theoretical predictions of the dCS gravity. The Love-Q relation measurement precision of our hierarchical Bayesian inference allows us to place a constraint on the dCS characteristic length $\xi_{\rm CS}^{1/4} < \mathcal{O}(10^2)$km. This result is consistent with previous works [11, 13] and highlights the power of the Love-Q relation inference for testing gravity theories.

Acknowledgments

References

[1] J.M. Lattimer and M. Prakash, *Neutron Star Observations: Prognosis for Equation of State Constraints*, *Phys. Rept.* **442** (2007) 109 [astro-ph/0612440].

[2] K. Hebeler, J.M. Lattimer, C.J. Pethick and A. Schwenk, *Equation of state and neutron star properties constrained by nuclear physics and observation*, *Astrophys. J.* **773** (2013) 11 [1303.4662].

[3] J. Antoniadis et al., *A Massive Pulsar in a Compact Relativistic Binary*, *Science* **340** (2013) 6131 [1304.6875].

[4] Lindblom, Lee, *Determining the Nuclear Equation of State from Neutron-Star Masses and Radii*, *Astrophys. J.* **398** (1992) 569.

[5] A.W. Steiner, J.M. Lattimer and E.F. Brown, *The Equation of State from Observed Masses and Radii of Neutron Stars*, *Astrophys. J.* **722** (2010) 33 [1005.0811].

[6] F. Ozel, G. Baym and T. Guver, *Astrophysical Measurement of the Equation of State of Neutron Star Matter*, *Phys. Rev. D* **82** (2010) 101301 [1002.3153].

[7] B.D. Lackey and L. Wade, *Reconstructing the neutron-star equation of state with gravitational-wave detectors from a realistic population of inspiralling binary neutron stars*, *Phys. Rev. D* **91** (2015) 043002 [1410.8866].

[8] P.T.H. Pang, I. Tews, M.W. Coughlin, M. Bulla, C. Van Den Broeck and T. Dietrich, *Nuclear Physics Multimessenger Astrophysics Constraints on the Neutron Star Equation of State: Adding NICER's PSR J0740+6620 Measurement*, *Astrophys. J.* **922** (2021) 14 [2105.08688].

[9] E. Berti et al., *Testing General Relativity with Present and Future Astrophysical Observations*, *Class. Quant. Grav.* **32** (2015) 243001 [1501.07274].

[10] L. Shao and K. Yagi, *Neutron stars as extreme laboratories for gravity tests*, *Sci. Bull.* **67** (2022) 1946 [2209.03351].

[11] K. Yagi and N. Yunes, *I-Love-Q*, *Science* **341** (2013) 365 [1302.4499].

[12] H.O. Silva, A.M. Holgado, A. Cárdenas-Avendaño and N. Yunes, *Astrophysical and theoretical physics implications from multimessenger neutron star observations*, *Phys. Rev. Lett.* **126** (2021) 181101 [2004.01253].

[13] K. Yagi and N. Yunes, *I-Love-Q Relations in Neutron Stars and their Applications to Astrophysics, Gravitational Waves and Fundamental Physics*, *Phys. Rev. D* **88** (2013) 023009 [1303.1528].

[14] LIGO Scientific, Virgo collaboration, *GW170817: Observation of Gravitational Waves from a Binary Neutron Star Inspiral*, *Phys. Rev. Lett.* **119** (2017) 161101 [1710.05832].

[15] LIGO Scientific, Virgo collaboration, *GW170817: Measurements of neutron star radii and equation of state*, *Phys. Rev. Lett.* **121** (2018) 161101 [1805.11581].

[16] LIGO Scientific, Virgo collaboration, *Properties of the binary neutron star merger GW170817*, *Phys. Rev. X* **9** (2019) 011001 [1805.11579].

[17] T. Hinderer, *Tidal Love numbers of neutron stars*, *Astrophys. J.* **677** (2008) 1216 [0711.2420].

[18] T. Damour and A. Nagar, *Relativistic tidal properties of neutron stars*, *Phys. Rev. D* **80** (2009) 084035 [0906.0096].

[19] J. Vines, E.E. Flanagan and T. Hinderer, *Post-1-Newtonian tidal effects in the gravitational waveform from binary inspirals*, *Phys. Rev. D* **83** (2011) 084051 [1101.1673].

[20] M. Favata, *Systematic parameter errors in inspiraling neutron star binaries*, *Phys. Rev. Lett.* **112** (2014) 101101 [1310.8288].

[21] L. Wade, J.D.E. Creighton, E. Ochsner, B.D. Lackey, B.F. Farr, T.B. Littenberg et al., *Systematic and statistical errors in a bayesian approach to the estimation of the neutron-star equation of state using advanced gravitational wave detectors*, *Phys. Rev. D* **89** (2014) 103012 [1402.5156].

[22] L. Baiotti, *Gravitational waves from neutron star mergers and their relation to the nuclear equation of state*, *Prog. Part. Nucl. Phys.* **109** (2019) 103714 [1907.08534].

[23] K. Chatziioannou, *Neutron star tidal deformability and equation of state constraints*, *Gen. Rel. Grav.* **52** (2020) 109 [2006.03168].

[24] E.E. Flanagan and T. Hinderer, *Constraining neutron star tidal Love numbers with gravitational wave detectors*, *Phys. Rev. D* **77** (2008) 021502 [0709.1915].

[25] J.B. Hartle and K.S. Thorne, *Slowly Rotating Relativistic Stars. II. Models for Neutron Stars and Supermassive Stars*, *Astrophys. J.* **153** (1968) 807.

[26] W.G. Laarakkers and E. Poisson, *Quadrupole moments of rotating neutron stars*, *Astrophys. J.* **512** (1999) 282 [gr-qc/9709033].

[27] E. Poisson, *Gravitational waves from inspiraling compact binaries: The Quadrupole moment term*, *Phys. Rev. D* **57** (1998) 5287 [gr-qc/9709032].

[28] I. Harry and T. Hinderer, *Observing and measuring the neutron-star equation-of-state in spinning binary neutron star systems*, *Class. Quant. Grav.* **35** (2018) 145010 [1801.09972].

[29] A. Samajdar and T. Dietrich, *Waveform systematics for binary neutron star gravitational wave signals: Effects of spin, precession, and the observation of electromagnetic counterparts*, *Phys. Rev. D* **100** (2019) 024046 [1905.03118].

[30] A. Abac, T. Dietrich, A. Buonanno, J. Steinhoff and M. Ujevic, *New and robust gravitational-waveform model for high-mass-ratio binary neutron star systems with dynamical tidal effects*, *Phys. Rev. D* **109** (2024) 024062 [2311.07456].

[31] M. Agathos, J. Meidam, W. Del Pozzo, T.G.F. Li, M. Tompitak, J. Veitch et al., *Constraining the neutron star equation of state with gravitational wave signals from coalescing binary neutron stars*, *Phys. Rev. D* **92** (2015) 023012 [1503.05405].

[32] N.V. Krishnendu, K.G. Arun and C.K. Mishra, *Testing the binary black hole nature of a compact binary coalescence*, *Phys. Rev. Lett.* **119** (2017) 091101 [1701.06318].

[33] N.V. Krishnendu, M. Saleem, A. Samajdar, K.G. Arun, W. Del Pozzo and C.K. Mishra, *Constraints on the binary black hole nature of GW151226 and GW170608 from the measurement of spin-induced quadrupole moments*, *Phys. Rev. D* **100** (2019) 104019 [1908.02247].

[34] Z. Lyu, M. LaHaye, H. Yang and B. Bonga, *Probing spin-induced quadrupole moments in precessing compact binaries*, *Phys. Rev. D* **109** (2024) 064081 [2308.09032].

[35] D. Reitze et al., *Cosmic Explorer: The U.S. Contribution to Gravitational-Wave Astronomy beyond LIGO*, *Bull. Am. Astron. Soc.* **51** (2019) 035 [1907.04833].

[36] D. Reitze et al., *The US Program in Ground-Based Gravitational Wave Science: Contribution from the LIGO Laboratory*, *Bull. Am. Astron. Soc.* **51** (2019) 141 [1903.04615].

[37] M. Punturo et al., *The Einstein Telescope: A third-generation gravitational wave observatory*, *Class. Quant. Grav.* **27** (2010) 194002.

[38] S. Hild et al., *Sensitivity Studies for Third-Generation Gravitational Wave Observatories*, *Class. Quant. Grav.* **28** (2011) 094013 [1012.0908].

[39] B. Sathyaprakash et al., *Scientific Objectives of Einstein Telescope*, *Class. Quant. Grav.* **29** (2012) 124013 [1206.0331].

[40] LIGO Scientific, Virgo collaboration, *GW170817: Implications for the Stochastic Gravitational-Wave Background from Compact Binary Coalescences*, *Phys. Rev. Lett.* **120** (2018) 091101 [1710.05837].

[41] B.S. Sathyaprakash et al., *Extreme Gravity and Fundamental Physics*, 1903.09221.

[42] V. Kalogera et al., *The Next Generation Global Gravitational Wave Observatory: The Science Book*, 2111.06990.

[43] A. Samajdar, J. Janquart, C. Van Den Broeck and T. Dietrich, *Biases in parameter estimation from overlapping gravitational-wave signals in the third-generation detector era*, *Phys. Rev. D* **104** (2021) 044003 [2102.07544].

[44] A. Samajdar and T. Dietrich, *Constructing Love-Q-Relations with Gravitational Wave Detections*, *Phys. Rev. D* **101** (2020) 124014 [2002.07918].

[45] I. Mandel and R. O'Shaughnessy, *Compact Binary Coalescences in the Band of Ground-based Gravitational-Wave Detectors*, *Class. Quant. Grav.* **27** (2010) 114007 [0912.1074].

[46] I. Mandel, *Parameter estimation on gravitational waves from multiple coalescing binaries*, *Phys. Rev. D* **81** (2010) 084029 [0912.5531].

[47] M.R. Adams, N.J. Cornish and T.B. Littenberg, *Astrophysical Model Selection in Gravitational Wave Astronomy*, *Phys. Rev. D* **86** (2012) 124032 [1209.6286].

[48] I. Mandel, W.M. Farr and J.R. Gair, *Extracting distribution parameters from multiple uncertain observations with selection biases*, *Mon. Not. Roy. Astron. Soc.* **486** (2019) 1086 [1809.02063].

[49] E. Thrane and C. Talbot, *An introduction to bayesian inference in gravitational-wave astronomy: Parameter estimation, model selection, and hierarchical models*, *Publications of the Astronomical Society of Australia* **36** (2019) .

[50] KAGRA, VIRGO, LIGO Scientific collaboration, *Population of Merging Compact Binaries Inferred Using Gravitational Waves through GWTC-3*, *Phys. Rev. X* **13** (2023) 011048 [2111.03634].

[51] Z. Wang, Y. Gao, D. Liang, J. Zhao and L. Shao, *Vetting quark-star models with gravitational waves in the hierarchical Bayesian framework*, *JCAP* **11** (2024) 038 [2409.11103].

[52] K. Yagi and N. Yunes, *Approximate universal relations for neutron stars and quark stars*, *Physics Reports* **681** (2017) 172.

[53] E. Thrane and C. Talbot, *An introduction to Bayesian inference in gravitational-wave astronomy: parameter estimation, model selection, and hierarchical models*, *Publ. Astron. Soc. Austral.* **36** (2019) e010 [1809.02293].

[54] J. Golomb and C. Talbot, *Hierarchical Inference of Binary Neutron Star Mass Distribution and Equation of State with Gravitational Waves*, *Astrophys. J.* **926** (2022) 79 [2106.15745].

[55] L.S. Finn, *Detection, measurement and gravitational radiation*, *Phys. Rev. D* **46** (1992) 5236 [gr-qc/9209010].

[56] N. Farrow, X.-J. Zhu and E. Thrane, *The mass distribution of Galactic double neutron stars*, *Astrophys. J.* **876** (2019) 18 [1902.03300].

[57] D. Atta, V. Singh and D.N. Basu, *Universal relationships for neutron stars from perturbative approach*, *New Astron.* **120** (2025) 102422 [2408.00646].

[58] Planck collaboration, *Planck 2018 results. VI. Cosmological parameters*, *Astron. Astrophys.* **641** (2020) A6 [1807.06209].

[59] M. Fishbach, D.E. Holz and W.M. Farr, *Does the Black Hole Merger Rate Evolve with Redshift?*, *Astrophys. J. Lett.* **863** (2018) L41 [1805.10270].

[60] LIGO Scientific, Virgo collaboration, *GW190425: Observation of a Compact Binary Coalescence with Total Mass* $\sim 3.4 M_\odot$, *Astrophys. J. Lett.* **892** (2020) L3 [2001.01761].

[61] N. Christensen and R. Meyer, *Markov chain Monte Carlo methods for Bayesian gravitational radiation data analysis*, *Phys. Rev. D* **58** (1998) 082001.

[62] N. Christensen, R.J. Dupuis, G. Woan and R. Meyer, *A Metropolis-Hastings algorithm for extracting periodic gravitational wave signals from laser interferometric detector data*, *Phys. Rev. D* **70** (2004) 022001 [gr-qc/0402038].

[63] J. Skilling, *Nested Sampling*, *AIP Conf. Proc.* **735** (2004) 395.

[64] J. Skilling, *Nested sampling for general Bayesian computation*, *Bayesian Analysis* **1** (2006) 833.

[65] C. Talbot and E. Thrane, *Flexible and Accurate Evaluation of Gravitational-wave Malmquist Bias with Machine Learning*, *Astrophys. J.* **927** (2022) 76 [2012.01317].

[66] M.J. Williams, J. Veitch, C. Chapman-Bird and R. Tenorio, *mj-will/nessai: v0.14.0.post0*, Jan., 2025. 10.5281/zenodo.14627250.

[67] M.J. Williams, J. Veitch and C. Messenger, *Nested sampling with normalizing flows for gravitational-wave inference*, *Phys. Rev. D* **103** (2021) 103006.

[68] M.J. Williams, J. Veitch and C. Messenger, *Importance nested sampling with normalising flows*, *Mach. Learn. Sci. Tech.* **4** (2023) 035011 [2302.08526].

[69] G. Ashton et al., *BILBY: A user-friendly Bayesian inference library for gravitational-wave astronomy*, *Astrophys. J. Suppl.* **241** (2019) 27 [1811.02042].

[70] N. Yunes, X. Siemens and K. Yagi, *Gravitational-wave tests of general relativity with ground-based detectors and pulsar-timing arrays*, *Living Rev. Rel.* **28** (2025) 3.

[71] R. Jackiw and S.Y. Pi, *Chern-Simons modification of general relativity*, *Phys. Rev. D* **68** (2003) 104012 [gr-qc/0308071].

[72] T.L. Smith, A.L. Erickcek, R.R. Caldwell and M. Kamionkowski, *The Effects of Chern-Simons gravity on bodies orbiting the Earth*, *Phys. Rev. D* **77** (2008) 024015 [0708.0001].

[73] S. Alexander and N. Yunes, *Chern-Simons Modified General Relativity*, *Phys. Rept.* **480** (2009) 1 [0907.2562].

[74] T. Gupta, B. Majumder, K. Yagi and N. Yunes, *I-Love-Q Relations for Neutron Stars in dynamical Chern Simons Gravity*, *Class. Quant. Grav.* **35** (2018) 025009 [1710.07862].

[75] Y. Ali-Haimoud and Y. Chen, *Slowly-rotating stars and black holes in dynamical Chern-Simons gravity*, *Phys. Rev. D* **84** (2011) 124033 [1110.5329].

[76] K. Yagi, N. Yunes and T. Tanaka, *Slowly Rotating Black Holes in Dynamical Chern-Simons Gravity: Deformation Quadratic in the Spin*, *Phys. Rev. D* **86** (2012) 044037 [1206.6130].

[77] K. Yagi, L.C. Stein, N. Yunes and T. Tanaka, *Isolated and Binary Neutron Stars in Dynamical Chern-Simons Gravity*, *Phys. Rev. D* **87** (2013) 084058 [1302.1918].

[78] K. Yagi, L.C. Stein, N. Yunes and T. Tanaka, *Post-Newtonian, Quasi-Circular Binary Inspirals in Quadratic Modified Gravity*, *Phys. Rev. D* **85** (2012) 064022 [1110.5950].